THE JOURNAL OF PHYSICAL CHEMISTRY B

Article

pubs.acs.org/JPCB

Thermal Treatment Effect on the Structure and Property Change between Hydroxy-Containing Polyimides (HPIs) and Thermally Rearranged Polybenzoxazole (TR-PBO)

Chi Hoon Park,[†] Elena Tocci,*[,†] Young Moo Lee,[‡,§] and Enrico Drioli[†,§,∥]

[†]Institute on Membrane Technology, ITM-CNR, Via P. Bucci Cubo 17/C, Rende (CS), 87036, Italy

[‡]School of Chemical Engineering, Hanyang University, Seoul, 133-791, Korea

[§]WCU Department of Energy Engineering, College of Engineering, Hanyang University, Seoul, 133-791, Korea

[∥]Department of Chemical Engineering and Materials, University of Calabria, Via P. Bucci Cubo 42/A, Rende (CS), 87036, Italy

ABSTRACT: In this study, we report on the effect of thermal treatment on polyimide precursors (HPIs) and on the resulting thermally rearranged polybenzoxazole (TR-PBO) polymer membranes as investigated through the use of molecular dynamics (MD) simulations. For this purpose, we have first analyzed the structures of hydroxy-containing polyimides before thermal treatment and those of the thermally rearranged polybenzoxazoles after the thermal treatment, according to their temperature conditions. As expected, HPIs and TR-PBOs always show very limited motion of their polymer chains, indicated by the radius of gyration, due to their well-known thermal stability. In particular, the very rigid and stiff PBO linkages did not undergo significant change in their torsional angle distribution. On the other hand, in regards to intrachain movement, HPI chains were significantly affected by temperature. Their conformational changes were notably observed, which affected the distances between possible reaction sites, oxygen atoms in hydroxyl groups, and carbon atoms in the imido-ring. The free volume analysis, performed on both polymers and during thermal treatment, indicates that HPIs have a unimodal distribution of free volume areas, which partially coalesce in larger areas having, however, a relatively narrow size. Further, TR-PBO shows a bimodal cavity distribution, and after thermal treatment and TR reaction, the free volume structures in TR-PBO are maintained. The cavity size distributions determined by simulation were also consistent with free volume distributions determined by positron annihilation lifetime spectroscopy.

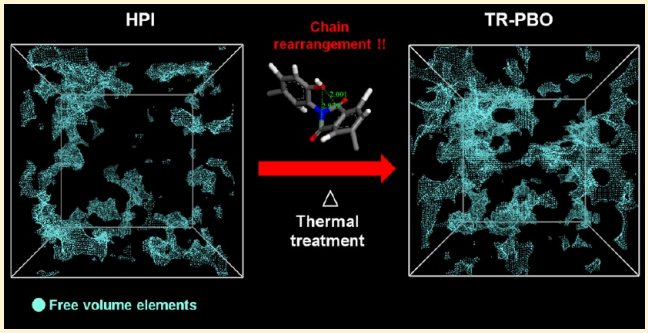

1. INTRODUCTION

The thermal treatment of polymers has been widely used to improve mechanical and chemical stability through physical effects such as annealing and quenching and/or chemical reactions such as cross-linking.[1−9] Thermally rearranged (TR)-polymers have been prepared from aromatic polymides containing ortho-positioned functional groups that, once thermally treated, rearrange into heteroaromatic polymers such as polyoxazoles, polybenzothiazole, polypyrrolone, and polybenzimidazole at temperatures higher than 350 °C.[10−12] These polymers show outstanding physical properties and high permeability that surpass the limits of conventional polymers due to unusual microstructures, which has been explained to be a result of the modifications of the polyimide chain during the rearrangement in the solid state structure; that is, rigid rods form with a concomitant randomization of conformations resulting from the formation of meta- and para-linked chains[10] and a modification of the free volume distribution.[13] However, it is difficult to demonstrate how thermal treatment affects polymer structure at the atomistic and molecular levels, specifically in terms of configuration, conformation, glass transition temperature, or free volume. In particular, if a chemical reaction occurs during the thermal treatment, the structure−property relationship between the starting and final structures become more and more complex.

In addressing this issue, modeling based on molecular dynamics (MD) and Monte Carlo simulation (MC) are regarded as powerful tools. Molecular modeling techniques have also provided a deeper understanding of the correlations between the structural features and transport of polymeric membrane materials.[14−21] Structural factors, such as conformation, configuration, and free volume topologies, can be specifically analyzed and intuitively demonstrated using MD simulations. As a result, MD simulations have been extensively used to investigate these features.[11,22] Consequently, molecular modeling can enhance our knowledge about membrane structure and properties. This fact, coupled with increasing

Received: July 25, 2012
Revised: September 17, 2012
Published: October 10, 2012

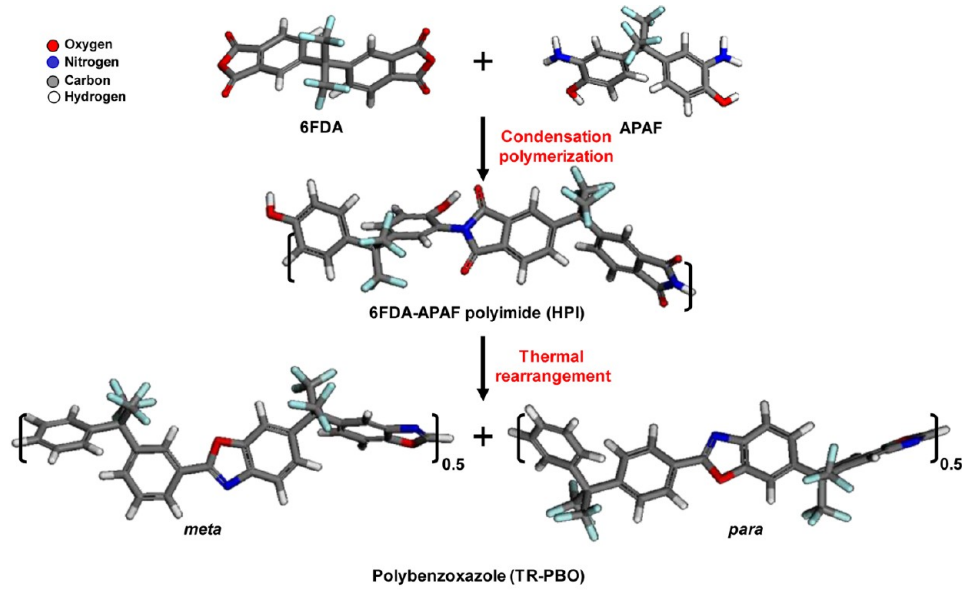

(a)

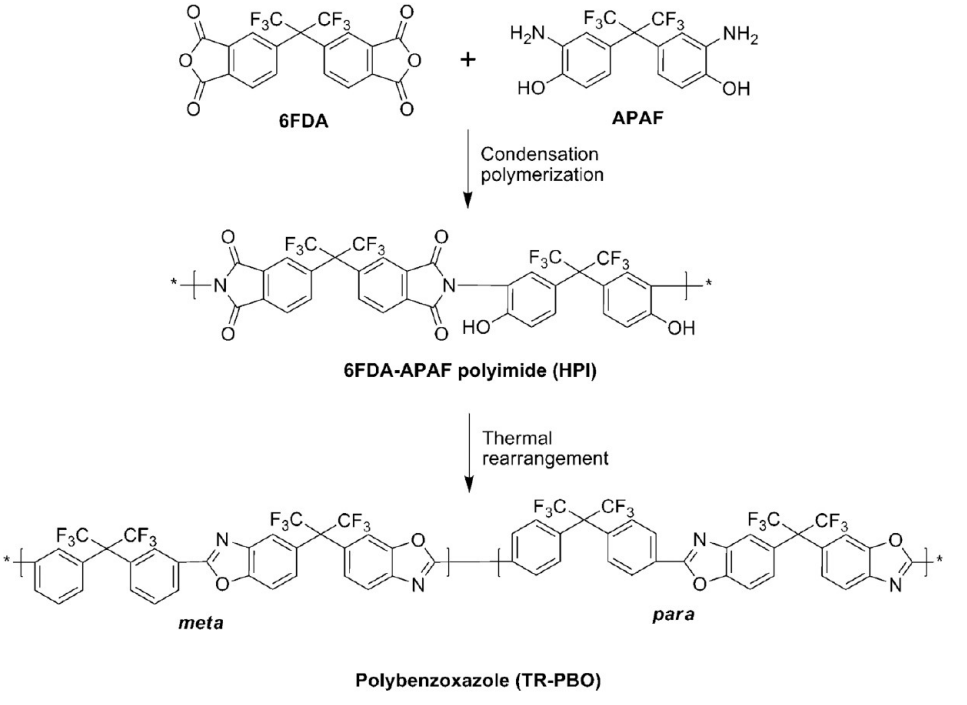

(b)

Figure 1. (a) Atomistic model and (b) chemical structure of hydroxyl-containing polyimide (HPI) and thermally rearranged polybenzoxazole (TR-PBO).

computational power and efficiency, allows macromolecular design to be brought to a wider range of users.

However, although polyimides (PIs) and polybenzoxazoles (PBOs) have received attention as promising engineering polymers due to their strong mechanical and chemical stabilities, there are not many reports dealing with thermal rearrangement reactions due to the problems presented by the rigidity of their cyclic backbone structures and the resulting complexity and difficulty in simulation. In terms of thermal treatment methods, the reaction that rearranges aromatic polymides into heteroaromatic polymers is one of the most complex and difficult mechanisms, since both physical and chemical aspects should be considered due to the high thermal treatment temperature required.[12]

This paper provides a detailed molecular modeling study on HPIs and TR-PBOs: we carried out atomistic simulations to analyze the structure of hydroxy-containing polyimides (HPIs) before the thermal treatment and of thermally rearranged

dx.doi.org/10.1021/jp307365y | J. Phys. Chem. B 2012, 116, 12864−12877

Table 1. Simulation Model Details and Final Properties

simulation models										simulated properties	
polymer	monomer	mole ratio	$\#_{chains}$	$\#_{repeat\ unit}$	$\#_{atoms}$	$M_{molecule}$	torsion[a]	$\#_{cell}$	name	density (g/cm^3)	cell size (Å)
HPI	6FDA-APAF	N/A	3	33	2246	25559.5	random	25	R25	1.4859 ± 0.0003	44.087 ± 0.003
								43	R43	1.4909 ± 0.0004	44.038 ± 0.004
							90°	44	90−44	1.4938 ± 0.0003	44.009 ± 0.003
								45	90−45	1.4867 ± 0.0004	44.079 ± 0.004
							180°	35	180−35	1.4910 ± 0.0003	44.037 ± 0.003
								49	180−49	1.4895 ± 0.0004	44.051 ± 0.004
TR	meta-PBO/para-PBO	5:5	3	33	2048	22654.9	random	8	R8	1.3810 ± 0.0004	43.396 ± 0.005
								47	R47	1.3803 ± 0.0007	43.403 ± 0.007
							90°	15	90−15	1.3808 ± 0.0005	43.398 ± 0.006
								47	90−47	1.3853 ± 0.0008	43.351 ± 0.008
							180°	24	180−24	1.3822 ± 0.0004	43.394 ± 0.005
								28	180−28	1.3832 ± 0.0006	43.372 ± 0.007

[a]The restriction of torsion angle was chosen at the polymer building steps.

polybenzoxazoles (TR-PBOs) after thermal treatment (see Figure 1). More importantly, the simulations were performed in a broad range of temperatures, starting from 25 to 450 °C for HPIs, and in opposite direction from 450 to 25 °C for TR-PBO, to elucidate the effect of temperature on the polymeric materials. The thermal movement of the polymeric chains and the resulting free volume and its distributions are analyzed, and the average cavity size is compared with those from PALS simulations.

2. SIMULATION DETAILS

2.1. Preparation of Amorphous Cells. Simulations of the amorphous cells of membranes have been carried out using the Material Studio (5.0) package of Accelrys[23] and the COMPASS force field[24,25] with two adjusted parameters: oxygen atoms in PBO rings modified from o2a (oxygen, SP2, aromatic, in a 5-membered ring) to o (oxygen, generic) and nitrogen atoms in PBO rings modified from n2a (nitrogen, SP2, aromatic) to n3a (nitrogen, SP2, aromatic).[13] COMPASS is an ab initio force field that enables accurate and simultaneous prediction of gas-phase properties (structural, conformational, vibrational, etc.) and condensed-phase properties (equation of state, cohesive energies, etc.) for a broad range of small molecules and polymers.[24,25]

After constructing single repeat units with charge groups assigned and subsequent energy minimization, isolated initial chain configurations of HPIs and TR-PBOs were constructed with various torsional angles of both HPI and PBO. The energy minimization step removes the unreal high internal energy of polymer chain including torsional energy, and finally modify the structure to become realistic polymer configuration. Details are summarized in Table 1. Synthetically, to prepare 6FDA-APAF polyimide, 4,4′-hexafluoroisopropylidene diphthalic anhydride (6FDA) and 2,2′-bis(3-amino-4-hydroxyphenyl)-hexafluoropropane (bisAPAF) are used. The theoretical procedure starts with building first HPI and PBO monomers. The next step is the preparation of polymer chains of HPI and PBO. Specifically, (1) for the construction of HPI chains: after preparing atomistic repeating units of the hydroxyl (6FDA-APAF) polyimide, a single atactic homopolymer chain with 33 repeat units (2246 atoms) was constructed; (2) for the construction of PBO chains: meta- and para-linked PBO monomers were prepared. Then, a single atactic copolymer chain with the appropriate molar ratio of m-PBO and p-PBO of 5:5 was constructed, using conditional statistics. The chains were constructed of 33 repeating units (2048 atoms).

For the packing procedure, a general methodology for generating realistic models of membranes has been used which consists of four steps: (1) the "initial packing," where the polymer chain and spacer molecules were packed in an amorphous cell at a lower density (about 10% of the final density). The spacer molecules were added randomly in the simulation box before the packing of the polymer was started to represent obstacles preventing the respective growing polymer chains from ring catenations and spearings. The obstacle molecules were later removed. (2) Each removal procedure was followed by energy minimization and MD runs combined with the "scaling" of conformation energy terms and nonbonded interaction energy terms in the force field. (3) A set of MD runs were performed to increase the density, and (4) longer MD runs were performed for the final equilibration. We built in total 300 models. Per each polymer type, that is, HPI and TR, 150 boxes have been constructed considering 50 boxes per each torsion restriction. After model validation, 6 boxes for HPI and 6 boxes for TR-PBO were chosen for this study. The applied techniques of packing and equilibration have been described in detail elsewhere.[26]

The initial packing procedure, Step 1, was performed with three atactic chains of 33 repeating units (a total of 6738 atoms and 7856 atoms for HPI and PBO chains, respectively, each chain having the same torsional angle) at a density lower than the experimental density. It can be assumed that, for stiff chain polymers, the effects of spatial nonuniformity would not be captured when modeling with relatively short chains. The cubic basic volume element was first filled with segments of a growing chain under periodic boundary conditions following a combination of the Theodorou−Suter[27,28] chain-generation approach and Meirovitch's scanning method,[29] thus reproducing the natural distribution of conformation angles. Since PIs and PBO contain cyclic subunits in the repeating units, the chain packing stage has to be performed at very low densities to avoid ring-catenation. To solve this technical problem, it is usually necessary to insert "solvent" molecules in the initial phase of the amorphous cell construction to avoid ring-catenation.

In this study, we have further optimized the idea of solvent inclusion in generating the amorphous cells. During the initial packing, we inserted the polymer chains as well as 200 methanol and 600 argon spacer molecules. Solvent was

dx.doi.org/10.1021/jp307365y | J. Phys. Chem. B 2012, 116, 12864−12877

removed in four steps, each step removing 200 molecules. After each step, several cycles of initial energy minimization was performed, followed by a brief NVT (constant number of particles, volume, and temperature) run at 303 K, and a final energy minimization step. After the elimination of the last set of argon atoms, the NVT run, and energy minimization, the density of the generated cells corresponded to nearly 90% of the experimental value. We have introduced a descriptor of the "goodness" of each packing attempt at an intermediary stage of construction: the variation of accessible volume (AV) to accessible surface area (ASA) ratio and its gradient, with the probe radius used to calculate the accessible volume and surface of each amorphous cell. The accessible volume for a probe of radius R is defined as the volume in the polymer matrix traced out by the probe's center for all of the regions in which the probe can fit. The accessible surface area and accessible volume were calculated with the Free Volume utility of the Visualizer module of the Material Studio (5.0) software package[23] using the accessible mode together with the fine grid spacing specifications, which will be further discussed in Section 2.2c. After the elimination of the nonrealistic boxes, we finally generated three realistic amorphous cells for each of the polymers.

Besides checking the quality of the boxes at an intermediate stage, we reached the experimental density by increasing the pressure with several cycles of NPT-MD (constant number of particle, temperature and pressure) runs at pressures of thousands of bars. Moreover, simulated annealing runs with temperatures up to 800 K and NVT dynamics at 303 K were used to further relax the polymeric structures. Equilibration and density adjustment of the polymer system were achieved through a final 300 ps MD run.

It is worth noting that small deviations in obtaining the experimental density may occur for glassy stiff-chain polymer materials,[14−16] particularly if the models are large.

2.2. Structural Characterization.

(a) The molecular conformation behavior of polymer chains is analyzed by calculating the radius of gyration (R_g), which gives a sense of the size of the polymer coil and is defined as:

$$R_g = \langle R_g^2 \rangle = \frac{1}{N} \langle \sum_{N}^{i=1} |\boldsymbol{r}_i - \boldsymbol{r}_{cm}|^2 \rangle \quad (1)$$

where $\boldsymbol{r}_i$ and $\boldsymbol{r}_{cm}$ represent the position vector of the ith atom and the center of mass of the polymer chain, respectively. The radius of gyration is also the quantity that is experimentally accessed.

(b) The radial distribution function (RDF) indicates the local probability density of finding B atoms at a distance r from A atoms averaged over the equilibrium density, as follows:

$$\mathrm{RDF}(r) = \frac{n_B/4\pi r^2 dr}{N_B/V} \quad (2)$$

where n_B is the number of B atoms at a distance r in a shell of thickness dr from atom A, N_B is the total number of B atoms in the system, and V is the total volume of the system.

(c) The fractional free volume (FFV) has also been used to characterize the final models. The theoretical values were compared with that of Bondi's group contribution method.[30]

The FFV is the ratio of the free volume, V_f, of a polymer (cm^3/g) and the specific volume, V_{sp}, defined as reciprocal density:

$$\mathrm{FFV} = \frac{V_f}{V_{sp}} \quad (3)$$

According to the Bondi method, the free volume can be estimated as:

$$V_f = V_{sp} - 1.3V_{vdW} \quad (4)$$

where the van der Waals volume V_{vdW} is calculated using a group contribution method, and a universal "packing coefficient", equal to 1.3, is used to convert the van der Waals volume of the repeat unit into the "occupied" volume.

In this work, free volume distributions were carried out using the Visualizer module of the Material Studio (5.0) software package.[23] First, the van der Waals surface is defined as the surface that intersects with the vdW radii of the atoms in the given structure, where the volume on the atom side of the surface (occupied volume) is used as the van der Waals volume. Based on the van der Waals surface, the accessible solvent surface is also defined as the surface that is the locus of the probe center as the probe rolls over the scaled vdW surface. This surface describes a space which could, in principle, be occupied by a probe of the given radius and is only defined over externally accessible regions, where the volume on the side of the surface without atoms (the free volume) is used as the accessible free volume.

A second computer program developed by Hofmann and Heuchel[31] was applied to estimate the size distributions of the free volume elements accessible for penetrants of certain radius. This process gives more accurate information than the original semiempirical group contribution method for determining the occupied volume. This free volume is determined by first superimposing a fine grid over the cubic packing; then a test is performed at every point of the grid to determine if an overlap occurs between a hard sphere test particle (representing the penetrating molecule) and any atom of the polymer (represented also by a corresponding hard sphere). The result is a classification of grid points as "occupied" or "free". Next, the connectivity of the "free" grid points is considered, and connected "free" grid points are collected into groups, which represent individual holes. This is done in two ways. In the first approach (named V connect), the topological criterion is that every point of a group has at least one next neighbor which is also member of this group. This approach identifies holes, which may be of complex shape and of large size. In a second approach, for every grid point, the shortest distance to a polymer atom is used to group points, and, among these distances, local maxima are defined by calculating the related gradient. Then, each grid point of the free-volume regions is assigned to its nearest local maximum. This approach is called R_{max}. Using this method, larger free-volume regions of elongated or highly complex shapes can be dissolved into smaller "local" regions, to come closer to the situation of PALS spectra, where the positron probe particle cannot completely sample very large holes of complex topology. The calculation starts by the superimposition of a fine grid of about 0.5 Å over the cubic packing model. In both approaches the number of lattice cells belonging to a hole times their cell volume was used

as a measure for the volume of this hole. The obtained volume of each hole was converted to an equivalent sphere. The radius of this sphere is taken as a measure for the average linear dimensions of the respective hole. The positronium (Posi) particle is assumed to have the size of a hydrogen atom; that is, the radius is assumed to be 1.10 Å.

3. RESULTS AND DISCUSSION

3.1. Thermal Effects. Thermal conversion of HPI into TR-PBOs occurs due to the attack of the hydroxide group to the adjacent amide carbonyl group. Figure 1 shows the synthetic route, starting from a dianhydride and diamine, and describes the currently proposed reaction pathway for thermal rearrangement.[11]

As proposed by Lee et al.,[10,11] after thermal rearrangement of a hydroxyl-imide ring to a carboxyl-benzoxazole intermediate, an aromatic bezoxazole ring is finally obtained by decarboxylation under thermal treatment in the range of 350−450 °C. However, since the thermal rearrangement is a complex and multistep process, this reaction has not been completely elucidated, and there has been some discussion regarding the process.[32,33] Lee et al. confirmed that thermal treatment of HPIs in the solid state leads to the formation of TR-PBOs. Thermal rearrangement kinetics seems to be faster in films than in powder samples. Mild thermal treatment conditions (i.e., low temperatures and short times) seem to result in negligible or low degrees of conversion to PBO.[34] In any case, the reaction route should be carefully considered to demonstrate the thermal treatment effect on the polymer structures of both HPI (precursor) and TR-PBO.

The thermal treatment of the TR reaction has a wide temperature range.[10,12] We performed this simulation following the experimental conditions at 298, 573, 623, 673, and 723 K for HPI and from 723 to 298 K for TR-PBO. The molecular dynamics (MD) simulation has an intrinsic limitation in that it calculates the motion of atoms at nanometer and nanosecond scales or less. For this reason, it is worth noting that this MD study could not reflect the final microstructure by the actual thermal rearrangement process, being caused by a reaction, but only the effect of the physical properties of materials.

Due to a large scattering of the data in the high temperature region of the energies/densities, it was necessary to calculate autocorrelation functions.[35] The scattering of the data is due to infrequent, large amplitude dihedral motions or dihedral flips that result in volume fluctuations. The autocorrelation function of these fluctuations was computed from a 500 ps run at 723 K. The functions converge to near zero between 200 and 250 ps. This means that 500 ps of simulation time at each temperature should be enough to reasonably describe the various states.

Table 2 shows the simulation protocol for thermal treatment modeling of HPIs and TR-PBOs. For this simulation, a total of nine boxes of HPIs and TR-PBOs were generated with three different structures per configuration with torsional angles of 90°, 180°, or a random angle. Finally, we chose two different structures from each configuration for the thermal treatment simulation. In total we analyzed six models for HPI and six for TR-PBO.

The fundamental question that arises relates to the way in which the thermal treatment affects the polymer chains of the HPI precursor and that of TR-PBO. To determine the answer, we investigated the effect of thermal treatment on the polymer chain distribution and movement.

Table 2. Temperature Steps for MD Simulation of HPIs and TR-PBOs

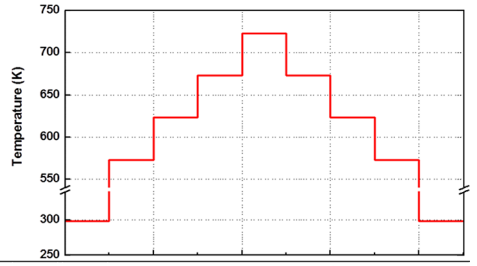

Polymer	Torsion angle	#	Temperature (K)								
			298	573	623	673	723	673	623	573	298
HPI	Random	25	→	→	→	→	→				
		43	→	→	→	→	→				
	90°	45	→	→	→	→	→				
		44	→	→	→	→	→				
	180°	35	→	→	→	→	→				
		49	→	→	→	→	→				
TR-PBO	Random	8					→	→	→	→	→
		47					→	→	→	→	→
	90°	47					→	→	→	→	→
		15					→	→	→	→	→
	180°	28					→	→	→	→	→
		24					→	→	→	→	→

We begin by examining how the molecular conformation behavior is affected by the thermal treatment along the HPI and TR-PBO chains. Figure 2 shows the radius of gyration of polymer chains in a 3D model of HPIs and TR-PBO. The different values depend on the torsional angles used to build the polymer chains. Random and 90° torsional angles produced more compact HPI polymers than a torsional angle of 180°. TR-PBO chains were less dependent on the initially given torsional angle because their strong rigidity restricted the final torsional angle distribution, revealing that the majority of the phenylene rings were about 30° from the oxazole units.

As temperature increases, polymers tend to have a wider distribution of the radius of gyration (R_g). For the same polymer, the larger the value of R_g, the more stretched out the polymer chain is. This indicates that the thermal vibrations cause a greater degree of stretching in the polymer chains. Here, both HPIs and TR-PBOs show very limited motion, which is not surprising due to their well-known thermal stability. However, in contrast with TR-PBOs, the R_g of HPIs starts to change at a thermal treatment temperature of 300 °C, and it is significantly visible at 450 °C. This indicates that HPI tend to be relatively unfolded. Also, the maximum peaks tend to shift from a lower to a higher radius of gyration, and the distribution is spread out over a larger peak. This result indicates that the HPI polymer coils are more enlarged.

Another indication of morphological behavior is given by the analysis of the torsional angles, as depicted in Figure 3. As already published,[10,11] the conformational change of HPI chains under thermal treatment affects the final porosity of TR-PBO due to formation of microvoids caused by chain disruption and rearrangement of stiff chains.

Figure 4 shows the torsional angles between the imide ring and the ortho-positioned hydroxyl-phenylene ring in HPI chains and between the phenyl ring and a benzoxazole ring in TR-PBO chains. Both dihedrals can be varied within a limited rotational energy barrier at a given temperature. The range of torsional angles is broadly distributed, revealing that phenylene rings are offset with the oxazole units, irrespective of the type of simulated amorphous HPI polymer cell. Since enough thermal energy enables the polymer chain to rotate over the torsional

dx.doi.org/10.1021/jp307365y | J. Phys. Chem. B 2012, 116, 12864−12877

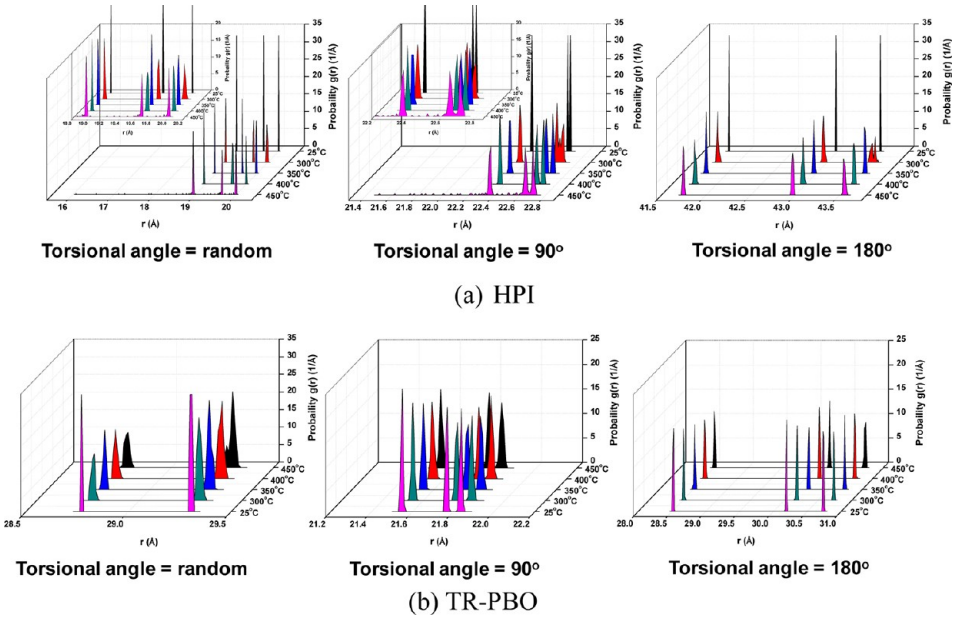

Figure 2. Change in the radius of gyration of 3D models of (a) HPIs and (b) TR-PBOs during thermal treatment simulations.

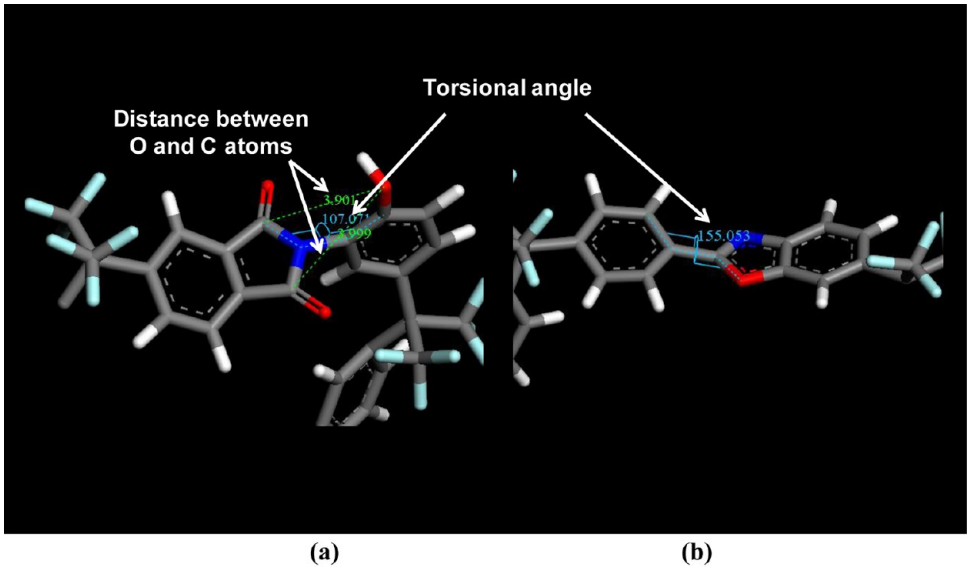

Figure 3. Schematic diagram of dihedral angles (C−N−Cph−CphOH) in HPI chain (a) and (Cph−Cph−C−O) PBO chain (b) for torsion distribution measurement (blue) and distances between the carbons in carboxyl groups of imido-linkage and the oxygen in hydroxyl groups of the opposite benzene ring in HPI chain (a) for length distribution measurement (green).

barrier energy, the distribution of HPI chains becomes flatter and more homogeneous with increasing temperature. The gray region in Figure 4a implies that the torsional angles of HPIs are closer to a meta-linkage than to a para-linkage, but the white region indicates the opposite. However, thermal motion makes the fluctuations wider. As a result, since HPIs are more flexible than TR-PBOs, this is reflected not only at 25 °C, but also at higher temperatures. It should be noted that the torsional angle distribution of HPI models in this study is rather complex compared with the monomer model study previously reported.[11] This can be explained by the complexity of conformations that can be found in a single polymer chain together with the statistical results averaged over three polymer chains. On the other hand, TR-PBO has a smaller range of distributions over all temperatures simulated due to the rigidity of the coplanar structure of the PBO ring, which is in accordance with the model study.[11]

The possible reaction sites should be verified to understand how a thermal treatment affects a thermal rearrangement reaction. HPIs are more flexible than PBOs, but the rigidity of HPIs is still quite high, and for this reason they are well-known for their thermal stability. For this reason, not many of the atoms in HPIs can participate in the reaction. In this work, because of the intrinsic limitations of MD simulation, we did not need to consider the whole reaction pathway during the thermal treatment, and instead we focused on the possible approaches of atoms involved in the chemical reaction, that is, the movement of hydroxyl groups and neighboring atoms as potential reaction sites. In particular, the carbons in the carboxyl groups of imide-linkage and the oxygen in hydroxyl

dx.doi.org/10.1021/jp307365y | J. Phys. Chem. B 2012, 116, 12864−12877

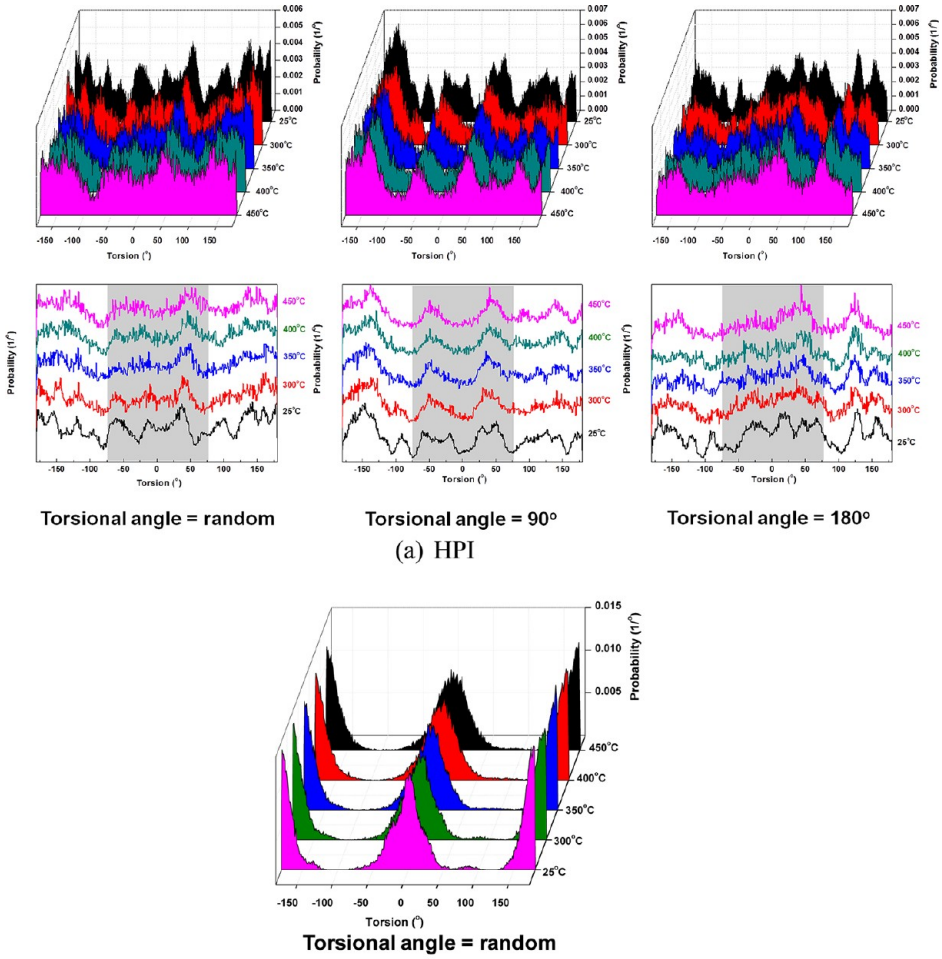

Figure 4. Change in the torsion distribution of 3D models of (a) HPIs and of (b) TR-PBO during thermal treatment simulations.

groups of the opposite benzene ring were chosen as possible actors of the reaction. Figure 5 shows the change in their distance under thermal treatment, which clearly demonstrates that the distances become closer and closer as temperature increases, decreasing to less than 2.3 Å at 450 °C. This could be an explanation for why 450 °C is so important for the TR reaction. Most of all, the increasing temperature increases the possibility of meta or para linkage formations in TR-PBO chains after the TR reaction, which is similar regardless of the torsional angles of the HPI chains. Along with the result from the torsion angle distribution test (Figure 4), this supports the assumption of a concomitant randomization of conformations in TR-PBO chains resulting from the formation of meta- and para-linked chains in the former papers.[10,11] Some examples are shown in Figure 6.

To investigate the distribution of linkages between carbon atoms in imide within a certain distance from oxygen atoms in hydroxyl groups, we analyzed the radial distribution functions (RDF) at various temperatures, as shown in Figure 7. The RDF indicates the probability density at which to find the distances between all of the corresponding atoms located through the 3D models. The results indicate that the first peaks lie in a range within 4 Å at 450 °C, with the peaks are shifted to the left, that is, to shorter distances, no matter the torsional angle used to construct the HPIs polymers. At long distances, the RDF approaches unity, which is not surprising for a purely amorphous system. The RDF diagrams suggest that, at high temperature, oxygen atoms in the hydroxyl groups tend to stay in proximity to the carbon atoms in imide moieties.

The RDF graph shows all possible interchain interaction sites. Accordingly, since the distance can be within 2.3 Å, similar to that shown in Figure 5, it seems possible to have an interchain TR reaction, although the total probability of this is much less than that of an intrachain TR reaction. A detailed analysis of selected snapshots indicates that, in some cases, the interchain distances between the reaction sites fall within 2.3 Å (Figure 8).

3.2. Free Volume Analysis. The most significant consequence of the thermal rearrangement of HPI to TR-PBO polymers is the change in the physical properties such as the fractional free volume (FFV). Indeed, the size and the distribution of the free volume regions in HPI and TR-PBO polymers are of great importance for the transport behavior of penetrant molecules. Generally, the precursor HPI membranes had very poor permeability similar to that of conventional fluorinated polyimides, but surprisingly, TR-PBO membranes exhibited superior gas permeability for small gas molecules.[12] Experimentally, the free volume has been characterized with positron annihilation lifetime spectroscopy (PALS),[10,12] and indirect information is given by the *d*-spacing values from the WAXD pattern.[13] Simulated atomistic bulk models have

dx.doi.org/10.1021/jp307365y | J. Phys. Chem. B 2012, 116, 12864−12877

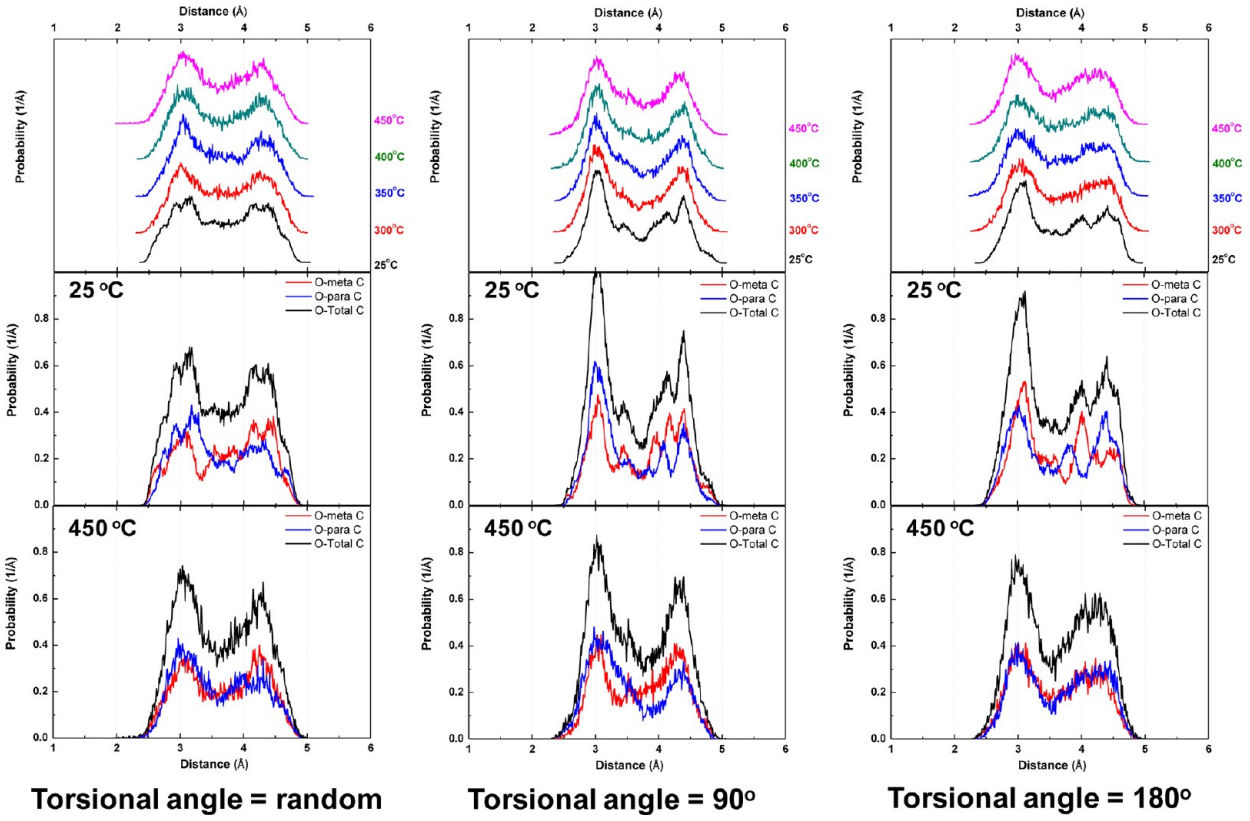

Figure 5. Change in distances between the reactive oxygen in the hydroxyl groups and the carbon in the imide linkages of HPIs during thermal treatment simulations.

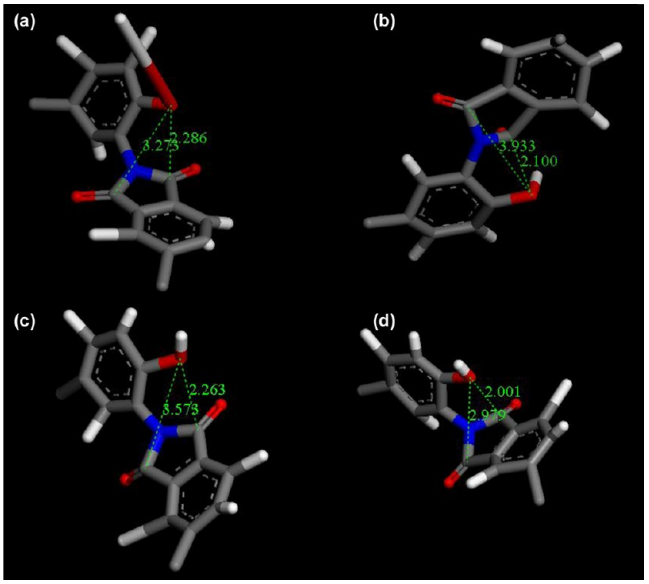

Figure 6. Simulation images of the 2.3 Å distance between the reactive oxygen in the hydroxyl groups and the carbon in the imide-linkages of HPIs with random torsion at 450 °C.

generally been used for accurate determination of geometrical quantities characterizing the structure of segmental packing.

Figure 9 shows a qualitative visualization of free volume elements for both HPI and TR-PBO packing models. The picture contains thin slices of about 5 Å thickness each perpendicular to the respective *z*-axis. A sphere of radius of 1.1 Å has been used as probe atoms representing the positronium-sized particle. The empty regions between the atoms indicate free volume elements. In Figure 9 the difference between the two polymers is visible. TR-PBO slices contain larger areas of free volume compared to HPI. This is in good agreement with the higher gas permeability polymers.[12] In TR-PBO the shape of the free volume elements in each slide is irregular and usually nonspherical. They are rather large, and some FVE elements may extend across several slices. This characteristic has already been found in high free volume polymers.[31,36,37,40]

The results of our free volume analysis are provided in Table 3. The fractional free volume (FFV) has been calculated using different methods, such as purely geometrically from the present packing models. Also, the Bondi data have been included in the table for comparison. As shown experimentally, differences in FFV are visible between HPIs and TR polymers, and both theoretical methods give higher values than that of Bondi's contribution method.

The analysis done with the Hofmann–Heuchel method[31] found an averaged accessible free volume of about 24451 Å^3 in HPI at 25 °C, corresponding to a FFV of 0.287. A similar value was found at 450 °C with a deviation in FFV of 2.14%. In TR-PBO, the FFV is generally higher (as expected from experimental data). At 25 °C, the accessible free volume is about 25 700 Å^3, corresponding to a FFV of 0.313. However, at 450 °C the accessible free volume is lower than the 1.02%, corresponding to a FFV of 0.310. These values are comparable to FFVs of amorphous fluoropolymers such as the Hyflon AD series,[36] although they are lower than that of the ultrahigh free volume polymer such as poly[1-(trimethylsilyl)-1-propyne] (PTMSP)[37] or than that of polymers with intrinsic microporosity (PIMs).[38−40]

dx.doi.org/10.1021/jp307365y | *J. Phys. Chem. B* 2012, 116, 12864−12877

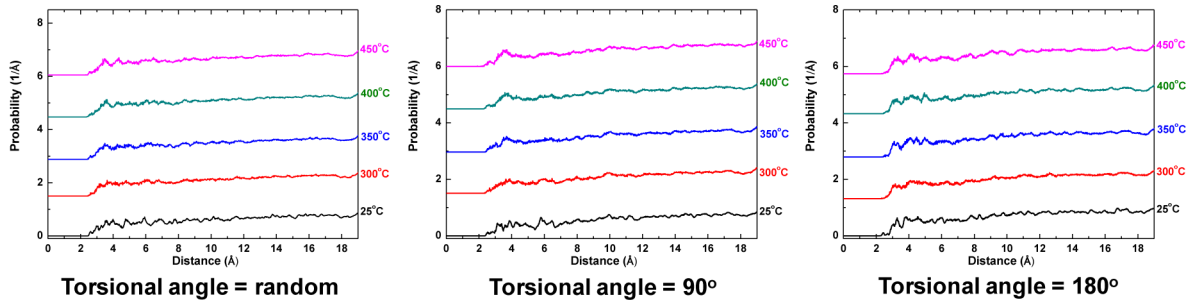

Figure 7. Change in the interchain distance between the reactive oxygen in the hydroxy groups of HPIs and the carbon in the imide linkage of the other HPIs during thermal treatment simulations.

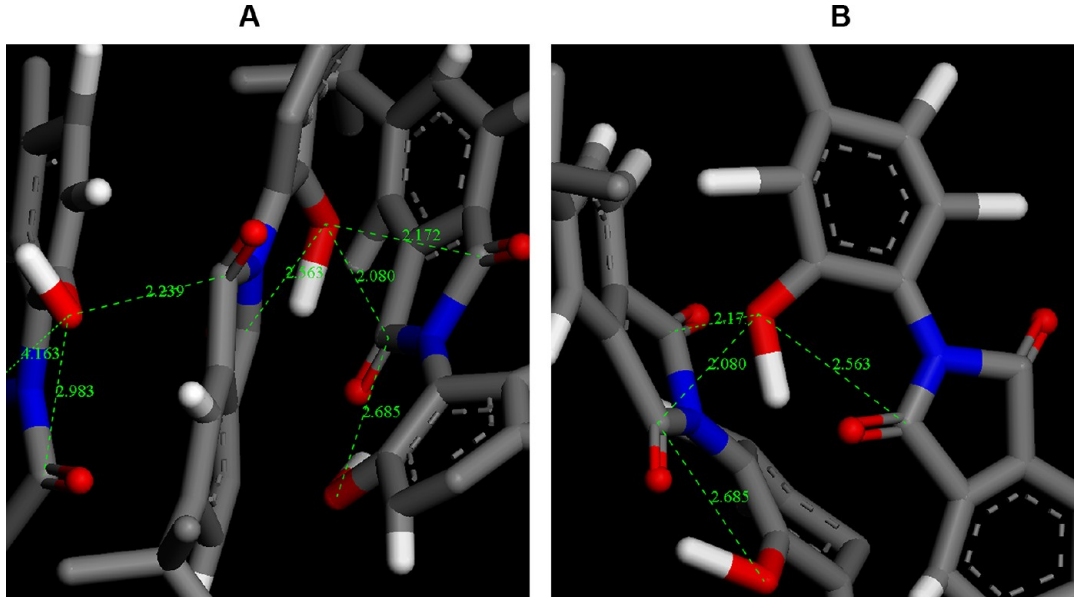

Figure 8. Simulation images with two different viewpoints of the interchain distance within 2.3 Å between the reactive oxygen in the hydroxyl groups and the carbon in the imide linkages of the HPIs with random torsion at 450 °C.

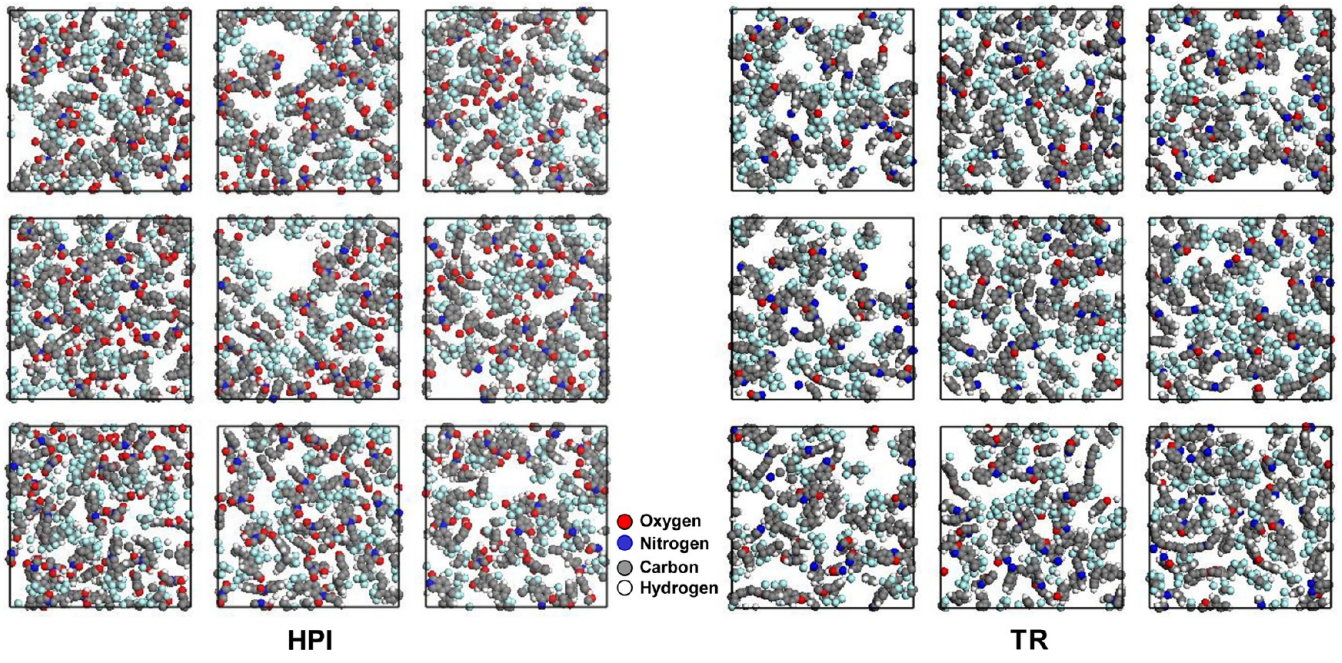

Figure 9. Representative slices of one packing model of HPI, thickness 4.8 Å (left) and of one packing model of TR-PBO, thickness 4.7 Å (right).

dx.doi.org/10.1021/jp307365y | J. Phys. Chem. B 2012, 116, 12864−12877

Table 3. Free Volume Analysis of HPIs and TR-PBOs

name	temp. (°C)	density (g/cm^3) simulated	fractional free volume calculated by Bondi's method[a]	van der Waals surface[b]	Hofmann–Heuchel method[c] (Rmax)	cavity radius calculated by PALS[d] small	large
HPI (R-43)	25	1.4911	0.17	0.214	0.287	3.37	
	300	1.4926		0.211			
	350	1.4893		0.213			
	400	1.4896		0.212			
	450	1.4901		0.213	0.281		
TR (R-8)	450	1.3819		0.250	0.296		
	400	1.3838		0.250			
	350	1.3841		0.250			
	300	1.3842		0.250			
	25	1.3841	0.22	0.251	0.303	1.76	4.190

[a]FFV = $(V - 1.3V_w)/V$. V is the molar volume of polymers (cm^3/mol). V_w is the van der Waals molar volume calculated by group contribution method.[12] [b]V_w is the simulated van der Waals molar volume in this study. FFV is calculated by the same equation of Bondi's method. [c]Hofmann group's R_{max} calculation with probe radius of 1.1 Å (the size of positronium in *J. Membr. Sci.* **2008**, *318*, 84[40]). [d]*Macromolecules* **2010**, *43*, 7657.[12]

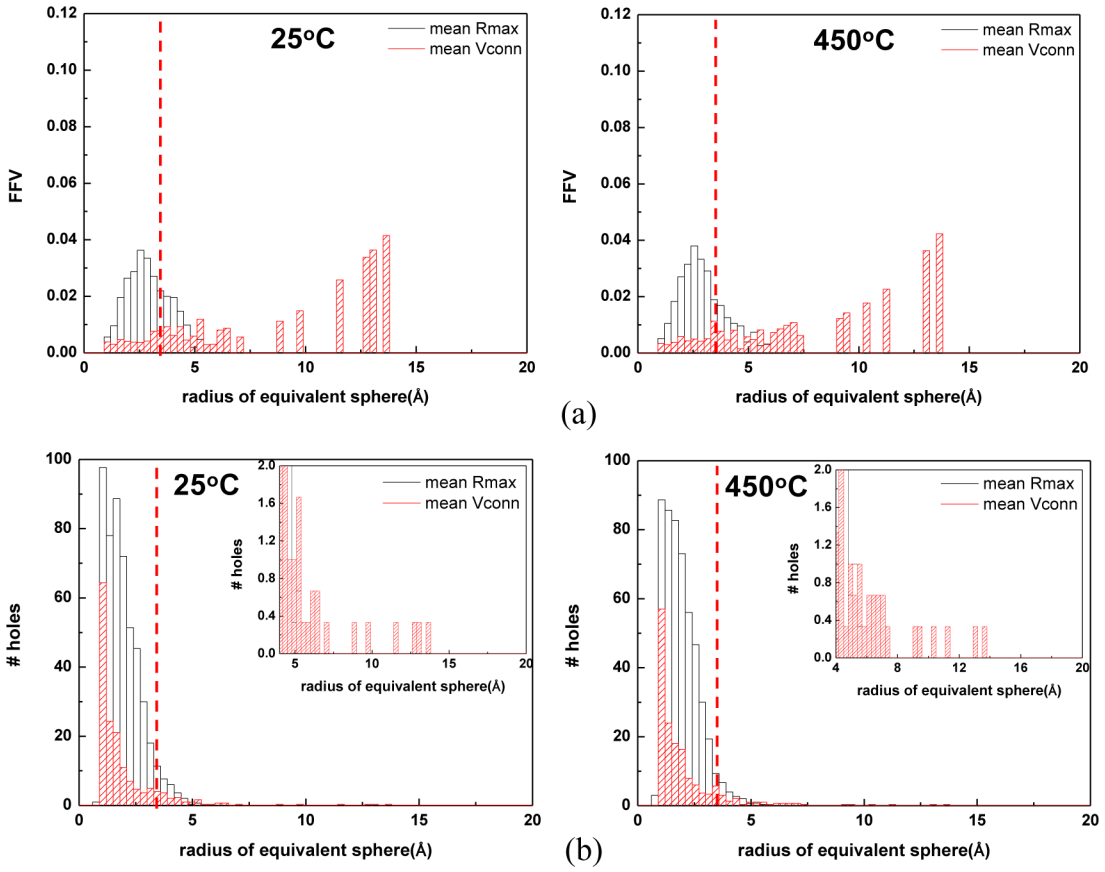

Figure 10. Cavity radius of free volume elements: bar-graph size distribution of (a) FVEs and (b) number of holes accessible for positronium calculated with the R_{max} (black) and $V_{connect}$ (red) approaches from packing models of HPIs before and after the thermal treatment. The dashed line represents the PALS data.[12]

Using the van der Waals surface method, the FFV was tested as a function of the thermal treatment. Because the free volume and the occupied volume depend on the temperature, it is expected that the FFV will likewise vary with the temperature. However, there was not a significant change in the quantity of free volume under the thermal treatment conditions investigated.

Considering the aforementioned morphological change in the polymer models, these unexpected results indicate the importance of the morphological analysis of free volume distribution as well as the amount of free volume to understand the effects of thermal treatment.

The size distributions of the free volume elements (FVEs) from the packing models have been calculated using the free volume probing method[31] using both the $V_{connect}$ and the R_{max} approach for every packing model. The last approach, with the distributions of fractional free volume elements accessible for

dx.doi.org/10.1021/jp307365y | *J. Phys. Chem. B* 2012, 116, 12864–12877

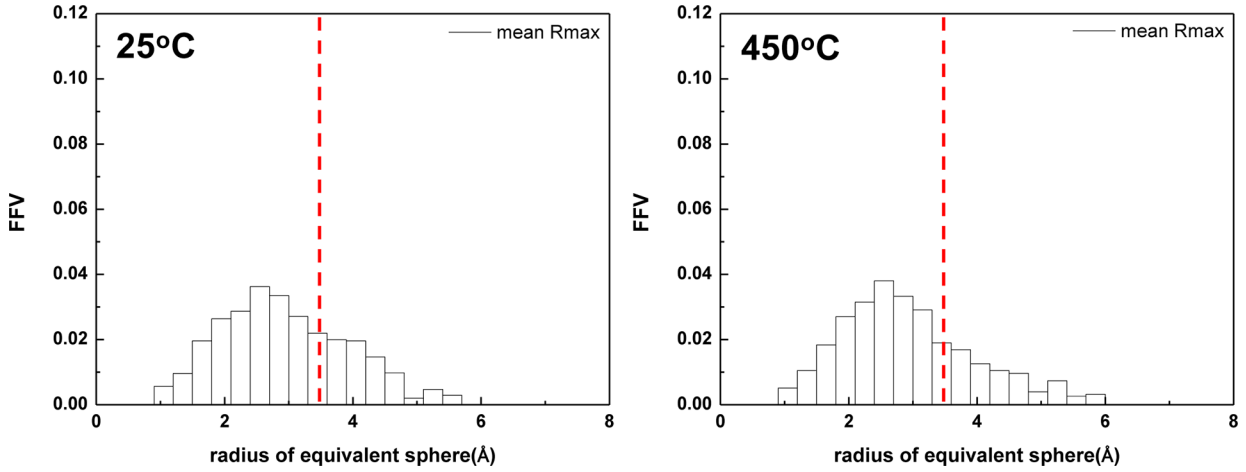

Figure 11. Cavity radius of free volume elements: bar-graph size distribution of free-volume elements accessible for Positronium calculated with the R_{max} approach from packing models of HPIs before and after the thermal treatment. The dashed line represents the PALS data.[12]

an *o*-positronium probe, is generally used for comparison with PALS data.[31,36]

Figure 10a and b shows the sizes distributions of the free volumes and the number of holes as an average of the HPI packing models in comparison with the results of the PALS data.[12] The $V_{connect}$ distribution shows peaks for equivalent sphere with apparent "radii" in a range up to 13 Å. It should be emphasized that the dimension of the radius does not imply that the packing model contains a single huge spherical hole of this size but indicates only the measure of the total extension of an interconnected free volume region. A similar spatial rearrangement of holes appears after thermal treatment: when any significant change in their geometric shape appears, this indicates an increased coalescence connectivity in the region between 5 Å and 10 Å to a larger amount of FFV. The peaks after 10 Å show almost the same radius.

The FVEs obtained by using the R_{max} approach show an unimodal distribution behaviors within 5.7 Å, which is in agreement with other PIs and PAIs[14] and with modified PEEK-WC[41] data that show the same distribution and relatively small sizes of free volume elements. The maximum of the distribution is at about 3.0 Å and agrees reasonable well with PALS measurements where an averaged radius of 3.37 Å was obtained according to the widely used accepted Tao-Eldrup model which assumes strictly spherical pores.[12]

In addition, a very small fraction of FVEs over 5 Å indicates that the dimensions of the free volume distributions in HPIs are not large (Figure 11). However, after thermal treatment, the fraction of FVE in this region partially increases. In the region between 4 and 6 Å the number of bars is more spread out, with a corresponding increase in each FFV bar. Since the total fraction of free volume does not change very much, as shown in Table 3, this can be explained by a coalescence of relatively small-sized free volume areas rather than a general thermal expansion of the free volume radius. This effect has also been observed by Lee et al.[10] from the analysis of PALS data as a function of treatment temperature. In that study, the authors observed an increase in mean cavity size with temperature, but a reduction in *o*-Ps intensity, meaning there was a decrease in the number of cavities, which suggested the coalescence of smaller cavities into larger ones.

Another significant effect of thermal rearrangement is the modification of internal surface area.[13] In this work, we used a kind of "shape factor", that is, the ratio between the volume and the surface, which can indicate variations in the contour of the free volume. Using the accessible solvent surface and volume calculation tools in the Accelrys software, we analyzed the volume/surface ratio with probes of increasing dimensions from 1.1 to 2 Å on HPI models at 25 and 450 °C. A higher volume/surface ratio is due to a higher volume or to a smaller surface. If there is a coalescence of two small free volume holes into a larger one, the surface of this hole is reduced. The curves shown in Figure 12 indicate that, above 1.6 Å, the volume/surface ratio diminishes at both temperatures, suggesting that the size of the free volumes with larger radii are reduced in number. However, the volume/surface ratio at a smaller radius, less than 1.6 Å, is much higher at 450 °C than at 25 °C. This indicates that a partial coalescence appears in the range between 1.2 and 1.4 Å, which confirms the behavior observed with the R_{max} approach. This provides evidence of an increase in size of larger pores obtained by more merging than occurs at lower temperatures.

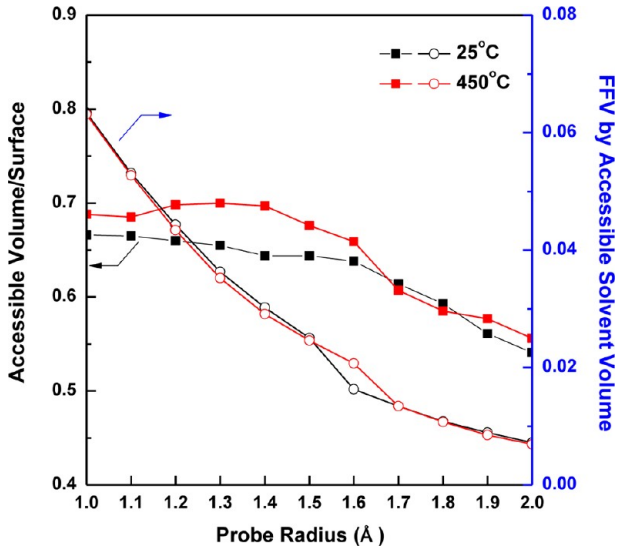

Figure 12. Thermal treatment effect on free volume and its morphology of HPI: ratio of accessible free volume to its surface area.

dx.doi.org/10.1021/jp307365y | J. Phys. Chem. B 2012, 116, 12864–12877

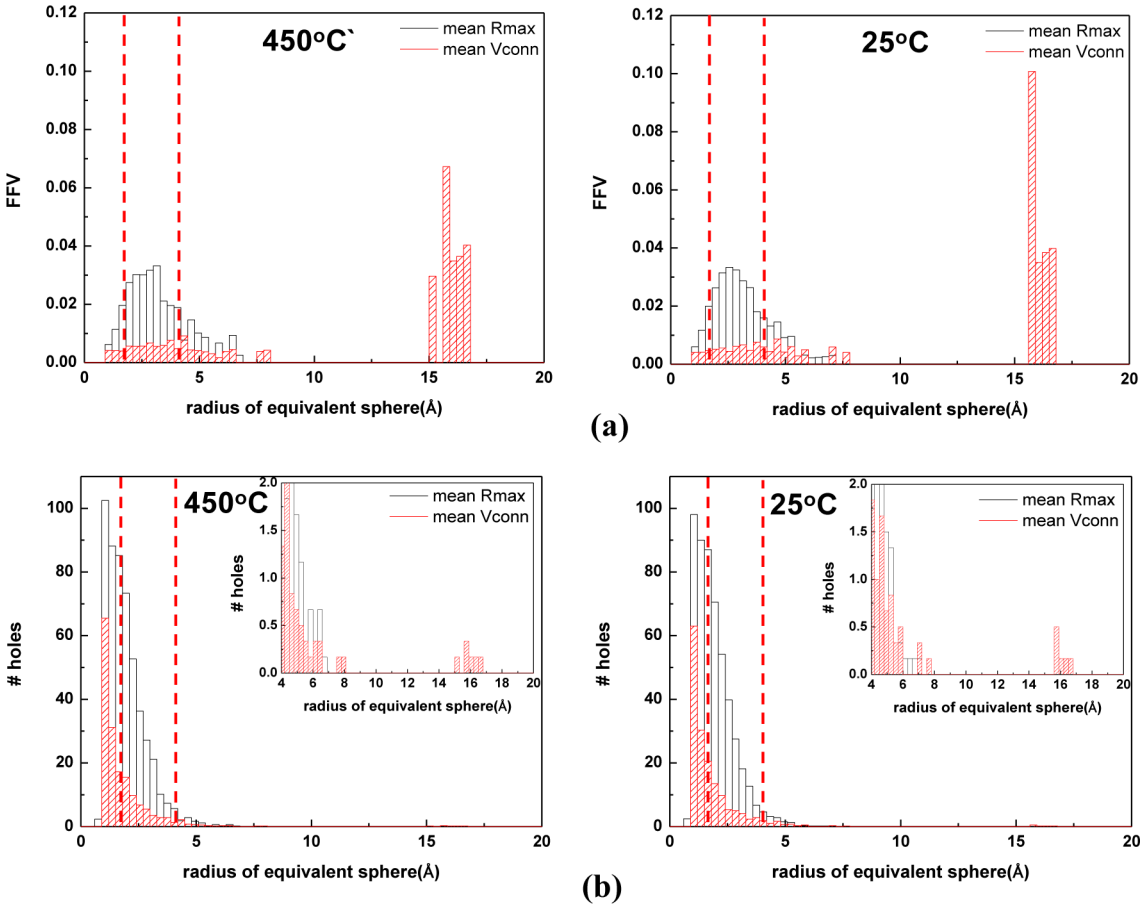

Figure 13. Cavity radius of free volume elements: bar-graph size distribution of (a) free-volume elements and (b) number of holes accessible for positronium calculated with the R_{max} (black) and $V_{connect}$ (red) approaches from packing models of TRs before and after the thermal treatment. The dashed line represents the PALS data.[12]

On the other hand, TR-PBO shows considerable differences in free volume analysis, yielding a much wider FVE bimodal distribution (Figure 13), with the $V_{connect}$ that broaden up to about 17 Å, which is the range found also for other high performance polymers.[31,36,37,40] The pseudomicroporous characteristics of thermally rearranged polymers[10] can be confirmed by comparison with the free volume analysis of PIM-1[40] polymer with intrinsic microporosity, for which $V_{connect}$ distributions extended up to about 1.7 nm and with the largest peaks of the FFV distribution at about 0.10−0.12. The difference with TR-PBO consists in the total amount of free volume, which is lower in TR-PBO. The outstanding performance of TR polymers, in comparison to HPI precursors, results from the large cavity formation caused by random chain conformations during thermal molecular rearrangement.[10]

For the R_{max} approach, additional distinct shoulders at cavity radii of about 6.0 Å have been found. In particular, the larger fraction of FVEs with a radius over 5 Å is much higher than that of the fraction found with HPI. This result is in good agreement with reports in previous literature that indicated that the intermolecular distances for TR polymers increased dramatically as confirmed by WAXD data of PBOs.[10−12] At 450 °C, TR-PBO behaves in similar manner to HPI. The free volumes in the range of the larger radii coalesce so that the fraction of FVE increases above 6 Å. The distribution obtained by MD is broader than the averaged PALS values and includes both peaks from the PALS experiments. It should be noted that the large FVEs of TR-PBO still remain after decreasing the temperature to 25 °C, confirming the higher rigidity of the polymer chains in comparison with the HPIs.

The volume/surface ratio in Figure 14a gives two indications: (1) the trend is similar for both temperatures, and (2) they are relatively constant, with only a small increase in the ratio, when the size of the probe increases. The relatively larger deviations between the two curves are in the range of 1.6 and 1.9 Å. The coalescence appears in the relatively larger free volume areas, as previously shown by the R_{max} approach. The constancy seems to indicate that the thermal treatment simply enlarges the smaller free volume zones. Figure 14b shows the connectivity of free volume; it is evident that it is also preserved at 25 °C.

Consequently, considering free volume analysis results of both HPI and TR-PBO, we can suggest the effects of thermal treatment on the free volume distribution during thermal rearrangement. First, as temperature increases, small free volumes in the HPI precursor are connected but still have a relatively small and narrow size. At 450 °C, thermal rearrangement occurs and creates large cavities around the imide linkages (i.e., PBO linkages after TR reaction) along the polymer chain due to deformation and formation of cyclic rings in the solid state and CO_2 evolution. These larger cavities could be connected with each other by the narrow free volumes generated during thermal treatment. Second, after thermal treatment and TR reaction, the connected free volumes in TR-PBO can keep their structures, even when the temperature decreases to 25 °C.

dx.doi.org/10.1021/jp307365y | J. Phys. Chem. B 2012, 116, 12864−12877

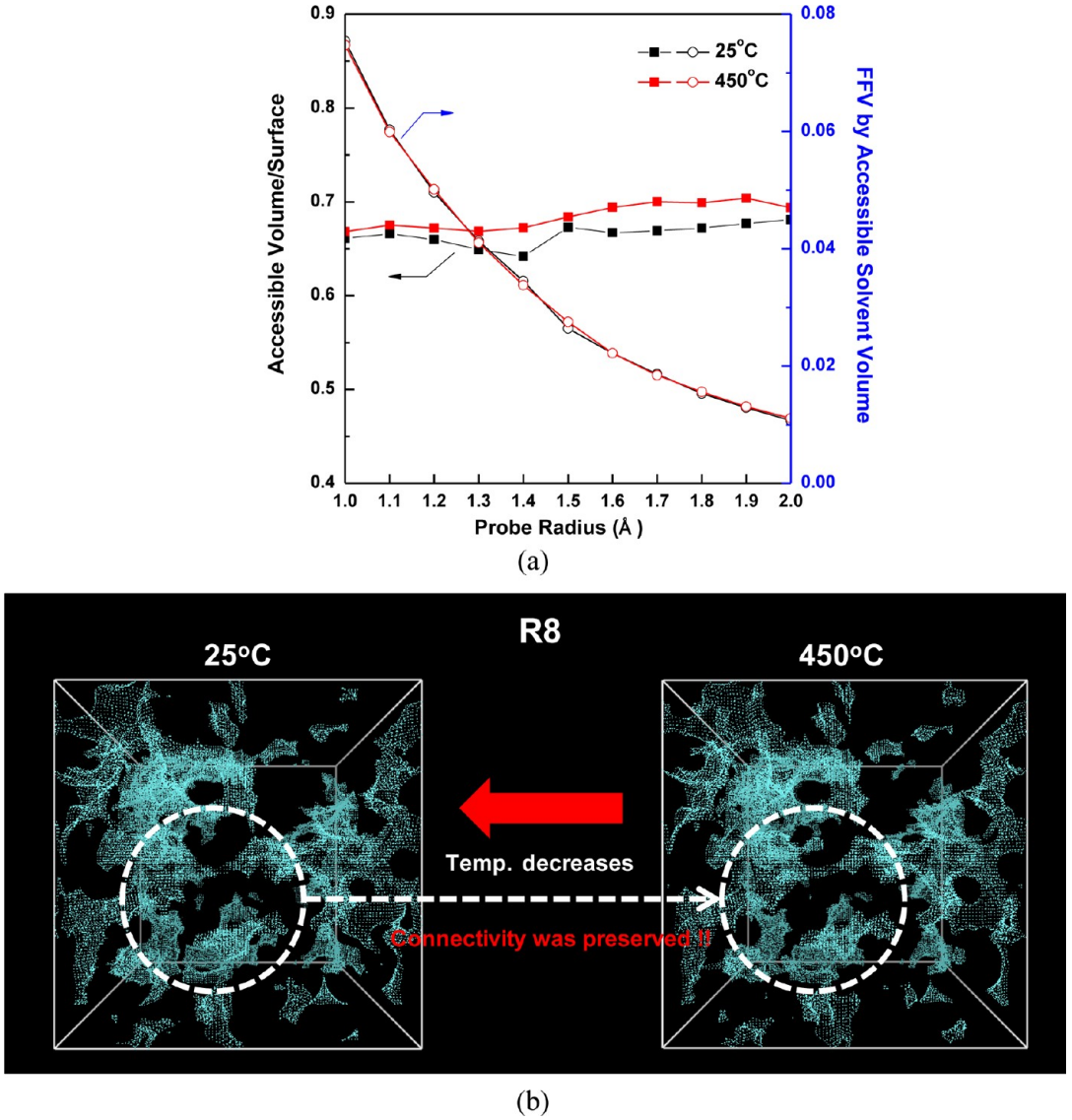

Figure 14. Thermal treatment effect on free volume and its morphology of TR: (a) ratio of accessible free volume to its surface area, (b) free simulated volume distribution image.

4. CONCLUSION

In this study, the effects of thermal treatment on the HPIs and TR-PBOs were investigated by MD simulations. The results indicate that the MD method could aid in understanding the effect of temperature on the thermal rearrangement reaction of HPIs to PBOs at the molecular level. According to the radius of gyration results of HPIs and TR-PBOs, both polymer chains showed very limited movement even at 450 °C due to their rigidity, which indicates that there is no change in bulk status such as melting and shrinkage under thermal treatment conditions if we do not consider reaction effects. On the other hand, for intrachain movement such as conformational change, each HPI and TR-PBO chain was affected by temperature but showed distinct differences. As temperature increased, the torsional angle distribution in HPI chains became homogeneous through the whole angle range from −180° to 180° due to the low torsional barrier energy of the imide linkage. However, very rigid and stiff PBO linkages did not change their torsional angle distribution significantly. Consequently, these different chain mobilities under the thermal treatment conditions contribute to the formation of peculiar free volume distributions and the morphology of TR-PBO, which is in good agreement with previously published studies.[10−12] The free volume analysis performed on HPI and TR-PBO during thermal treatment indicates that the unimodal distribution of HPIs partially coalesces in larger areas having relatively smaller and narrower sizes. At 450 °C, when the thermal rearrangement occurs, cavities became larger around the imide linkages that are the active sites of the TR reaction. TR-PBO shows a completely different cavity distribution such as the high-performance polymers (e.g., PIMs, PTMSP), and after thermal treatment, the connected free volumes in TR-PBO keep their structures even when the temperature decreases to 25 °C.

■ AUTHOR INFORMATION

Corresponding Author

*Tel.: +39-0984-49-2038. E-mail: e.tocci@itm.cnr.it.

Notes

The authors declare no competing financial interest.

■ ACKNOWLEDGMENTS

This work was supported in the framework of the NEMOPUR project (FP7 Marie Curie Actions ITN: Grant No. 214226-2). Y.M.L. and E.D. wish to acknowledge WCU (World Class University Program) through the National Research Foundation of Korea funded by Ministry of Education, Science and Technology (R31-10092), for the partial support to this work. Y.M.L. appreciates Korea Carbon Capture and Sequestration R&D Center under the Korea CCS 2020 program through the National Research Foundation of Korea funded by Ministry of Education, Science and Technology for financial support.

■ REFERENCES

(1) Choi, S. H.; Jansen, J. C.; Tasselli, F.; Barbieri, G.; Drioli, E. *Sep. Purif. Technol.* **2010**, *76*, 132−139.
(2) Hensley, J. E.; Way, J. D.; Dec, S. F.; Abney, K. D. *J. Membr. Sci.* **2007**, *298*, 190−201.
(3) Jeon, J. D.; Cho, B. W.; Kwak, S. Y. *J. Power Sources* **2005**, *143*, 219−226.
(4) Kanehashi, S.; Nakagawa, T.; Nagai, K.; Duthie, X.; Kentish, S.; Stevens, G. *J. Membr. Sci.* **2007**, *298*, 147−155.
(5) Park, C. H.; Lee, C. H.; Guiver, M. D.; Lee, Y. M. *Prog. Polym. Sci.* **2011**, *36*, 1443−1498.
(6) Park, H. B.; Shin, H. S.; Lee, Y. M.; Rhim, J. W. *J. Membr. Sci.* **2005**, *247*, 103−110.
(7) Duthie, X.; Kentish, S.; Pas, S. J.; Hill, A. J.; Powell, C.; Nagai, K.; Stevens, G.; Qiao, G. *J. Polym. Sci., Part B: Polym. Phys.* **2008**, *46*, 1879−1890.
(8) Maya, E. M.; Muñoz, D. M.; de la Campa, J. G.; de Abajo, J.; Lozano, Á. E. *Desalination* **2006**, *199*, 188−190.
(9) Meier-Haack, J.; Lenk, W.; Berwald, S.; Rieser, T.; Lunkwitz, K. *Sep. Purif. Technol.* **2000**, *19*, 199−207.
(10) Park, H. B.; Jung, C. H.; Lee, Y. M.; Hill, A. J.; Pas, S. J.; Mudie, S. T.; Van Wagner, E.; Freeman, B. D.; Cookson, D. J. *Science* **2007**, *318*, 254−258.
(11) Park, H. B.; Han, S. H.; Jung, C. H.; Lee, Y. M.; Hill, A. J. *J. Membr. Sci.* **2010**, *359*, 11−24.
(12) Han, S. H.; Misdan, N.; Kim, S.; Doherty, C. M.; Hill, A. J.; Lee, Y. M. *Macromolecules* **2010**, *43*, 7657−7667.
(13) Han, S. H.; Kwon, H. J.; Kim, K. Y.; Seong, J. G.; Park, C. H.; Kim, S.; Doherty, C. M.; Thornton, A. W.; Hill, A. J.; Lozano, A. E.; Berchtold, K. A.; Lee, Y. M. *Phys. Chem. Chem. Phys.* **2012**, *14*, 4365−4373.
(14) Heuchel, M.; Hofmann, D.; Pullumbi, P. *Macromolecules* **2004**, *37*, 201−214.
(15) Hofmann, D.; Fritz, L.; Ulbrich, J.; Schepers, C.; Bohning, M. *Macromol. Theory Simul.* **2000**, *9*, 293−327.
(16) Tocci, E.; Hofmann, D.; Paul, D.; Russo, N.; Drioli, E. *Polymer* **2001**, *42*, 521−533.
(17) Liivat, A.; Brandell, D.; Thomas, J. O. *J. Mater. Chem.* **2007**, *17*, 3938−3946.
(18) Greenwell, H. C.; Bowden, A. A.; Chen, B.; Boulet, P.; Evans, J. R. G.; Coveney, P. V.; Whiting, A. *J. Mater. Chem.* **2006**, *16*, 1082−1094.
(19) Brandell, D.; Liivat, A.; Aabloo, A.; Thomas, J. O. *J. Mater. Chem.* **2005**, *15*, 4338−4345.
(20) Hektor, A.; Klintenberg, M. K.; Aabloo, A.; Thomas, J. O. *J. Mater. Chem.* **2003**, *13*, 214−218.
(21) Park, C. H.; Lee, C. H.; Sohn, J.-Y.; Park, H. B.; Guiver, M. D.; Lee, Y. M. *J. Phys. Chem. B* **2010**, *114*, 12036−12045.
(22) Jiang, Y.; Willmore, F. T.; Sanders, D.; Smith, Z. P.; Ribeiro, C. P.; Doherty, C. M.; Thornton, A.; Hill, A. J.; Freeman, B. D.; Sanchez, I. C. *Polymer* **2011**, *52*, 2244−2254.
(23) Material Studio (5.0) package of Accelrys. *Polymer User Guide. Polymerizer section*; Accelrys Software Inc.: San Diego, 2009.
(24) Rigby, D.; Sun, H.; Eichinger, B. E. *Polym. Int.* **1997**, *44*, 311−330.
(25) Sun, H.; Rigby, D. *Spectrochim. Acta, Part A* **1997**, *153*, 1301−1323.
(26) Park, C. H.; Tocci, E.; Drioli, E. unpublished work.
(27) Theodorou, D. N.; Suter, U. W. *Macromolecules* **1985**, *18*, 1467−1478.
(28) Theodorou, D. N.; Suter, U. W. *Macromolecules* **1986**, *19*, 139−154.
(29) Meirovitch, H. *J. Chem. Phys.* **1983**, *79*, 502.
(30) Bondi, A. *J. Phys. Chem.* **1964**, *68*, 441−451.
(31) Hofmann, D.; Heuchel, M.; Yampolskii, Y.; Khotimskii, V.; Shantarovich, V. *Macromolecules* **2002**, *35*, 2129−2140.
(32) Hodgkin, J. H.; Dao, B. N. *Eur. Polym. J.* **2009**, *45*, 3081−3092.
(33) Hodgkin, J. H.; Liu, M. S.; Dao, B. N.; Mardel, J.; Hill, A. J. *Eur. Polym. J.* **2011**, *47*, 394−400.
(34) Calle, M.; Lozano, A.; Lee, Y. M. *Eur. Polym. J.* **2012**, *48*, 1313−1322.
(35) van der Vegt, N. F. A.; Briels, W. J.; Wessling, M.; Strathmann, H. *J. Chem. Phys.* **1999**, *110*, 11061−11069.
(36) Jansen, J. C.; Macchione, M.; Tocci, E.; De Lorenzo, L.; Yampolskii, Y. P.; Sanfirova, O.; Shantarovich, V. P.; Hofmann, D.; Drioli, E. *Macromolecules* **2009**, *42*, 7589−7604.
(37) Hofmann, D.; Entrialgo-Castano, M.; Lerbret, A.; Heuchel, M.; Yampolskii, Y. *Macromolecules* **2003**, *36*, 8528−8538.
(38) Ghanem, B. S.; McKeown, N. B.; Budd, P. M.; Fritsch, D. *Macromolecules* **2008**, *41*, 1640−1646.
(39) Du, N.; Robertson, G. P.; Pinnau, I.; Guiver, M. D. *Macromolecules* **2010**, *43*, 8580−8587.
(40) Heuchel, M.; Fritsch, D.; Budd, P. M.; McKeown, N. B.; Hofmann, D. *J. Membr. Sci.* **2008**, *318*, 84−99.
(41) Hofmann, D.; Tocci, E. Chapter 1. Molecular modeling. A tool for the knowledge-based design of polymer-based membrane materials. In *Membrane Operations: innovative separations and transformations*; Drioli, E., Giorno, L., Eds.; Wiley-VCH Verlag GmbH & Co. KGaA: Weinheim, Germany, 2009; Chapter 1, pp 253−255.